Energy and Resources Recovery from Reverse Osmosis Desalination Concentrate

Tushar Jain; PhD advisor: Haizhou Liu
Department of Chemical and Environmental Engineering, University of California, Riverside, CA

Research background and overview:

The overarching goal of this research project is to develop technologies for beneficial salinity management. Specifically, the project focuses on the energy and resources recovery from reverse osmosis (RO) desalination concentration, which can reduce the cost associated with desalination operation and minimize the environmental impact associated with the disposal of desalination concentrate. The project has been carried out in two phases. The first phase of the study emphasized on harvesting salinity energy from concentrate using an electrochemical capacitor system. The second phase investigated the resource recovery, specifically, phosphorus from RO concentration.

Phosphorous is a valuable element that is essential as a fertilizer in agricultural industry. However, it has been speculated that the world phosphorus production from phosphate rock will peak to its high in the decade of 2030-40 and then the production will inescapably decrease due to the depletion of its natural reserves. Due to the shrinking supply and ever increasing demand the quality of reserves is declining (Runge-Metzger, 1995). Florida is one of the leading producer of phosphorus in the United States (Jasinki, 2005) reported that the phosphate rock reserves in Florida, could be totally depleted by 2050. RO concentrate has a considerable level of organic phosphorous, mainly due to the application of phosphonate-based antiscalant. In membrane related desalination processes phosphorus-containing chemicals (*i.e.*, organophosphates) are used as antiscalants to prevent scaling of membranes. These antiscalants have excellent chelating properties and are also very effective inhibitor of mineral precipitation, thus raising the saturation point of sparingly soluble salts including calcium carbonate ($CaCO_3$), calcium sulfate ($CaSO_4$) and others. It is estimated that the concentration of organic phosphorous in the RO concentrate can reach several mg/L. This is a significant source of phosphorous. However, RO concentrate is typically discharged without recovering the phosphorous from organic phosphate in antiscalant. High phosphorus content due to concentrate disposal can lead to eutrophication in receiving water bodies and degradation of ecological system. For example, a phosphorous concentration as low as 30 μg/L can cause severe eutrophication. In addition, as excellent chelating agents, organic phosphonate compounds can mobilize potentially toxic metals in the receiving water.

Currently, little research has been done to investigate the potential to extract organic phosphonate from RO concentrate, convert it to inorganic phosphorous and recover as a valuable phosphate fertilizer. Technologies for removing phosphorus from the concentrate are still unexplored. Recovering the phosphonate in its antiscalant form has received some attention in the recent years (Mohammadesmaeili, 2010). However, no prior research has investigated the recovery of phosphate as an inorganic fertilizer.

In this research, we have studied different adsorbents to recover phosphates from the RO concentrate. Different type of iron oxides and sand have been used conventionally to adsorb

organics and various type of contaminants from aqueous solutions (Luo and Yao et al., 2016, Fard, Ahmad Kayvani, et al., 2016, Dadfarnia, S., et al., 2015). Specifically, iron oxides are known to be excellent adsorbents with a very high capacity of adsorption for phosphorus from water due to the strong binding properties (Cornell and Schwertmann, 2013). They have been successfully used as an adsorbent for arsenic removal from wastewater. This selective affinity of phosphorus to the surface of iron oxides gives it an edge over adsorption of other anions (Geelhoed et al., 1997 and Genz, 2005), mainly due to interactions of surface charges. Thus, our proposed approach involves the adsorption of organic phosphonate on the surface of an adsorbent from RO concentrate, subsequent desorption of the organic phosphonate from the iron oxide surface at an elevated pH to generate a concentrated solution. Following that, an advanced oxidation step using ultraviolet-based hydrogen peroxide (H_2O_2) was employed to convert organic phosphonate to value inorganic phosphorous mineral as fertilizer. We also looked at the impact of presence of different other contaminants such as presence of SO_4 on the adsorption of phosphate on iron oxides. The research objectives are to:

- Determine the extent of adsorption of antiscalant on sand.
- Study the efficacy of different type of iron oxides for the adsorption of antiscalant.
- Investigate the impact of presence of sulfate (SO_4) on the recovery of antiscalant.
- Perform theoretical calculations for determining the form of predominant mineral precipitated.

Results and discussion

Adsorption of antiscalant on sand:

Figure 1 shows concentration of the antiscalant, nitrilotris methylene triphosphonic acid (NTMP), in the solution during the process of adsorption. Adsorption was performed with various dosage

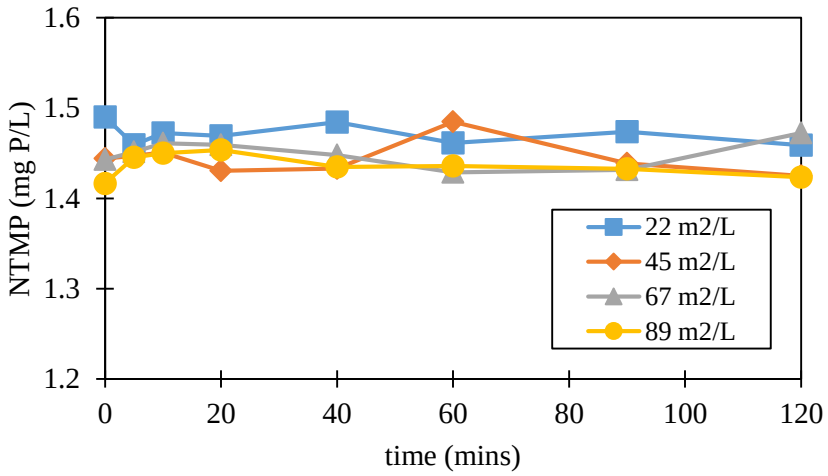

Figure 1: Adsorption of NTMP on various dosage of sand; adsorption pH: 7.8; NTMP dosage: 1.5 mg P/L

of sand with respect to time. It can be inferred from this figure that effectively, NTMP does not

adsorb on sand. In order to further investigate the adsorption of NTMP on other solids, adsorption experiments were performed on different iron oxides such as ferrihydrite and goethite and activated charcoal.

Adsorption on iron oxides:

Figure 2 shows the results from the adsorption of NTMP on goethite. The bars show the distribution of NTMP during the process of adsorption after the equilibrium is reached. The orange bar shows the fraction of the antiscalant left in the solution after the equilibrium is reached at pH 7.8. The blue and grey bar, together show the fraction of the antiscalant that gets adsorbed on the surface of the adsorbent. Once the solution pH is raised to pH 11.0, the antiscalant desorbs from

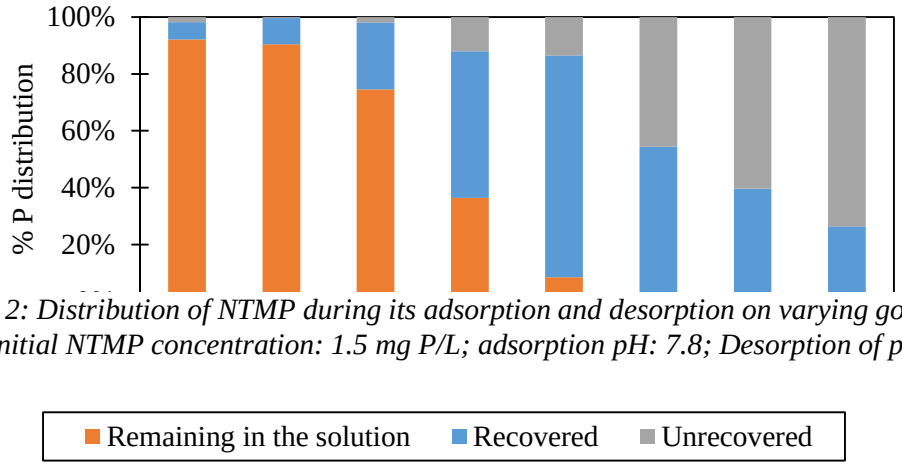

Figure 2: Distribution of NTMP during its adsorption and desorption on varying goethite dosage; initial NTMP concentration: 1.5 mg P/L; adsorption pH: 7.8; Desorption of pH: 11.0.

the surface and a new equilibrium is reached. Thus the blue portion shows the fraction of antiscalant that can be recovered (desorb) and the fraction that permanently adsorbs on the surface is shown by grey bar. Figure 2 above shows that with increasing dosage of adsorbent, the extent of adsorption of the antiscalant increases. However, the permanently unrecovered fraction also increases with the same. Thus there is an optimum dosage for the adsorbent for which the recovery

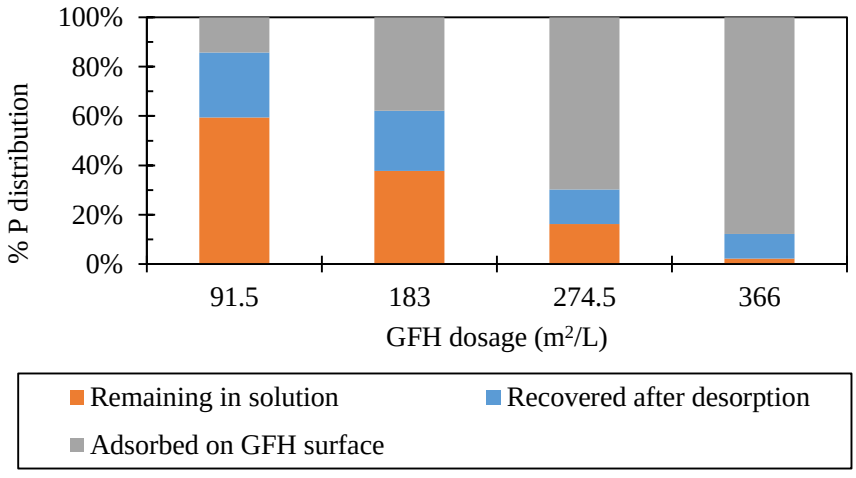

Figure 3: Distribution of NTMP during its adsorption and desorption on varying ferrihydrite dosage; initial NTMP concentration: 1.5 mg P/L; adsorption pH: 7.8; Desorption pH: 11.0

is maximum. Similar trend is seen for another form of iron oxide, ferrihydrite, but with much higher dosage of adsorbent. Also, the recovery is not as high as it is observed for goethite. The above results confirm that organic phosphorus in the form of antiscalants can be easily removed from the water matrix and can be recovered by changing the pH of the solution.

We hypothesize that the adsorption-desorption of the antiscalant on these iron oxides is an electrostatic phenomena which occurs due to the change in the surface charge due to the changing solution pH. NTMP has bulky electronegative phosphate groups which bonds with the adsorbent surface which is electropositive at pH 7.8. Thus it is important to study the impact of presence of other electronegative species which are present in considerable concentrations such as sulfate (SO_4^{-2}). Consistent with the previous studies, Boels et al., 2012, *figure 4* shows the impact of presence of varying concentrations of sulfate on the adsorption of NTMP on ferrihydrite. Similar

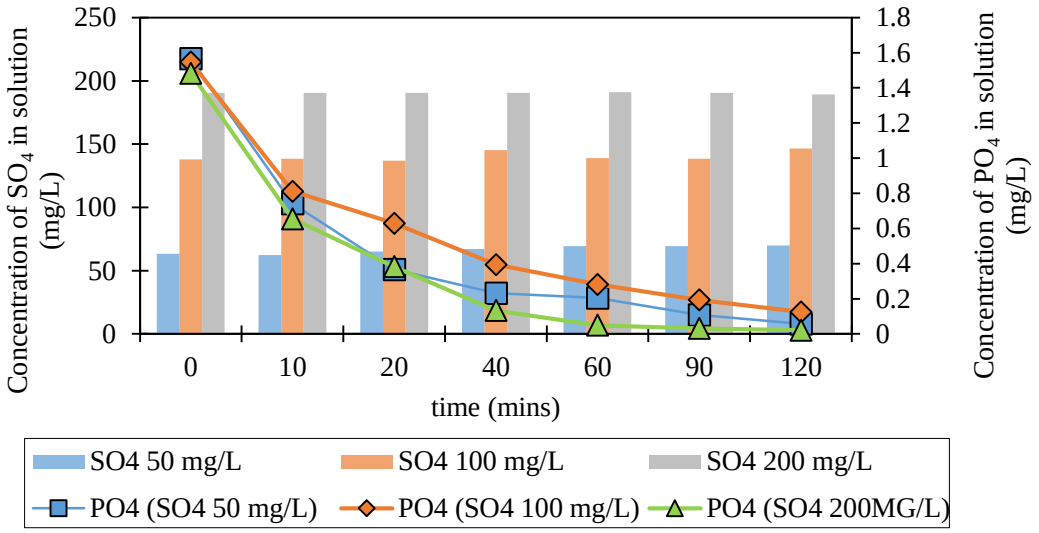

Figure 4: Adsorption profile of NTMP on ferrihydrite in presence of varying SO_4^{-2} dosage; adsorption pH 7.8

results as seen in *figure 5* were observed for adsorption of NTMP on goethite in the presence of varying sulfate dosage. The presence of sulfate seems to have no effect on the adsorption efficiency of either adsorbent. Sulfate does not adsorb on the adsorbent site, thus the antiscalant does not have to compete for the active sites on iron oxides for adsorption. Additional experiments were performed with goethite of different particle size and hence different normal surface area in order to observe the impact of particle size on the adsorption characteristics of antiscalant. However there was not much difference observed in the performance even with surface areas differing by more than an order of magnitude (20 m^2/L and 160 m^2/L).

Recovery of phosphorus as mineral:

Advanced oxidation of antiscalant will lead to the breakdown of organic antiscalant to its inorganic form. Thus, the water matrix will supersaturate leading to crystallization of Mg^{2+} and Ca^{2+} salts of the anions. These salts can be recovered in its pure form by simple separation process. RO

concentrate has high concentration of PO_4^{3-}, Cl^-, SO_4^{2-}, CO_3^{2-} and NH_4^+ anions. It is important to determine the salt that will precipitate out based on the equilibrium. Hence, we performed some theoretical calculations to determine the predominantly precipitating salts.

Table 1 and *Table 3* below show the various calcium and magnesium ligand species in water with their respective stability constants. Ligands considered for the present study includes PO_4^{3-}, Cl^-, SO_4^{2-}, CO_3^{2-} and NH_4^+. Equation (1) and equation (19) represent the mass balance for total calcium and total magnesium present in the system between its various possible aqueous species as described in *Table 1* and *Table 3* respectively with the ligands as described above.

Table 1: Stability constants for Ca- ligand complexes

	Metal ligand complexes	**LogK**
(i)	$Ca^{2+} + 2H^+ + PO_4^{3-} \leftrightarrow CaH_2PO_4^+$	20.923
(ii)	$Ca^{2+} + H^+ + PO_4^{3-} \leftrightarrow CaHPO_{4(aq)}$	15.035
(iii)	$Ca^{2+} + H_2O \leftrightarrow CaOH^+ + H^+$	-12.697
(iv)	$Ca^{2+} + PO_4^{3-} \leftrightarrow CaPO_4^-$	6.46
(v)	$Ca^{2+} + Cl^- \leftrightarrow CaCl^+$	0.4
(vi)	$Ca^{2+} + CO_3^{-2} \leftrightarrow CaCO_{3(aq)}$	3.22
(vii)	$Ca^{2+} + H^+ + CO_3^{2-} \leftrightarrow CaHCO_3^+$	11.434
(viii)	$Ca^{2+} + 2NH_4^+ \leftrightarrow Ca(NH_3)_2^{2+} + 2H^+$	-18.59
(ix)	$Ca^{2+} + NH_4^+ \leftrightarrow CaNH_3^{+2} + H^+$	-9.04

$$[TOTCa]_{diss} = Ca^{2+} + CaH_2PO_4^+ + CaH_2PO_{4(aq)} + CaOH^+ + CaPO_4^- + CaCl^+ + CaCO_{3(aq)} + CaHCO_3^+ + Ca(NH_3)_2^{2+} + CaNH_3^{+2} \quad (1)$$

$$[TOTCa]_{diss} = Ca^{2+}\left\{1 + \frac{CaH_2PO_4^+}{Ca^{2+}} + \frac{CaHPO_{4(aq)}}{Ca^{2+}} + \frac{CaOH^+}{Ca^{2+}} + \frac{CaPO_4^-}{Ca^{2+}} + \frac{CaCl^+}{Ca^{2+}} + \frac{CaCO_{3(aq)}}{Ca^{2+}} + \frac{CaHCO_3^+}{Ca^{2+}} + \frac{Ca(NH_3)_2^{2+}}{Ca^{2+}} + \frac{CaNH_3^{+2}}{Ca^{2+}}\right\} \quad (2)$$

$$[TOTCa]_{diss} = Ca^{2+}\left\{1 + K_1(H^+)^2(PO_4^{3-}) + K_2(H^+)(PO_4^{3-}) + \left(\frac{K_3}{(H^+)}\right) + K_4(PO_4^{3-}) + K_5(Cl^-) + K_6(CO_3^{-2}) + K_7(H^+)(CO_3^{-2}) + \frac{K_8(NH_4^+)^2}{(H^+)^2} + \frac{K_9(NH_4^+)}{(H^+)}\right\} \quad (3)$$

Where $[TotCa]_{diss}$ is the total soluble calcium concentration.

Table 2 contains the solubility product values for the solids of interest in our system. Equations (4-18) show the concentration of metal ions when their respective metal salt precipitates out.

Table 2: K_{sp} values for calcium solids

	Equilibrium speciation for solids	$LogK_{sp}$
(a)	$Ca_3(PO_4)_{2(am1)} \leftrightarrow 3Ca^{2+} + 2PO_4^{3-}$	-25.5
(b)	$Ca_3(PO_4)_{2(am2)} \leftrightarrow 3Ca^{2+} + 2PO_4^{3-}$	-28.25
(c)	$Ca_3(PO_4)_{2(beta)} \leftrightarrow 3Ca^{2+} + 2PO_4^{3-}$	-28.92
(d)	$Ca_4H(PO_4)_3.3H_2O \leftrightarrow 4Ca^{2+} + H^+ + PO_4^{3-}$	-47.95
€	$CaHPO_{4(s)} \leftrightarrow Ca^{2+} + H^+ + PO_4^{3-}$	-19.275
(f)	$CaHPO_4.2H_2O \leftrightarrow Ca^{2+} + H^+ + PO_4^{3-} + 2H_2O$	-18.995
(g)	$Ca_5(PO_4)_3(OH)_{(s)} \leftrightarrow 5Ca^{2+} + 3PO_4^{3-} + H_2O$	-44.333
(h)	$CaO + 2H^+ \leftrightarrow Ca^{2+} + H_2O$	32.6993
(i)	$Ca(OH)_2 \leftrightarrow Ca^{2+} + H_2O$	22.704
(j)	$CaCO_3 \leftrightarrow Ca^{2+} + CO_3^{2-}$	-8.336
(k)	$CaCO_3.H_2O \leftrightarrow Ca^{2+} + CO_3^{2-} + H_2O$	-7.144
(l)	$CaCO_3 \leftrightarrow Ca^{2+} + CO_3^{2-}$	-8.48
(m)	$CaCO_3 \leftrightarrow Ca^{2+} + CO_3^{2-}$	-7.913
(n)	$CaSO_4 \leftrightarrow Ca^{2+} + SO_4^{2-}$	-4.36
(o)	$CaSO_4.2H_2O \leftrightarrow Ca^{2+} + SO_4^{2-} + 2H_2O$	-4.63

$$Ca^{2+} = \left\{\frac{K_{sp1}}{\left(PO_4^{3-}\right)^2}\right\}^{\frac{1}{3}} \quad (4)$$

$$Ca^{2+} = \left\{\frac{K_{sp2}}{\left(PO_4^{3-}\right)^2}\right\}^{\frac{1}{3}} \quad (5)$$

$$Ca^{2+} = \left\{\frac{K_{sp3}}{\left(PO_4^{3-}\right)^2}\right\}^{\frac{1}{3}} \quad (6)$$

$$Ca^{2+} = \left\{\frac{K_{sp4}}{(H^+)\left(PO_4^{3-}\right)^3}\right\}^{\frac{1}{4}} \quad (7)$$

$$Ca^{2+} = \frac{K_{sp5}}{(H^+)(PO_4^{3-})} \quad (8)$$

$$Ca^{2+} = \frac{K_{sp6}}{(H^+)(PO_4^{3-})} \quad (9)$$

$$Ca^{2+} = \left\{\frac{K_{sp7}(H^+)}{\left(PO_4^{3-}\right)^3}\right\}^{\frac{1}{5}} \quad (10)$$

$$Ca^{2+} = K_{sp8}(H^+)^2 \quad (11)$$

$$Ca^{2+} = K_{sp9}(H^+)^2 \quad (12)$$

$$Ca^{2+} = \frac{K_{sp10}}{CO_3^{2-}} \quad (23)$$

$$Ca^{2+} = \frac{K_{sp11}}{CO_3^{2-}} \quad (14)$$

$$Ca^{2+} = \frac{K_{sp12}}{CO_3^{2-}} \quad (15)$$

$$Ca^{2+} = \frac{K_{sp13}}{CO_3^{2-}} \quad (16)$$

$$Ca^{2+} = \frac{K_{sp14}}{CO_4^{2-}} \quad (17)$$

$$Ca^{2+} = \frac{K_{sp15}}{CO_4^{2-}} \quad (18)$$

Figure 5 is plotted assuming that each solid precipitates individually with the total ligand concentration as described in the figure. It shows the equilibrium between the total concentration of the dissolved metal ion and the concentration of the ions in solid form. Usually for a concentrate water matrix, its pH will be in the range well within 5-10. *Figure 5* and *figure 6* show the predominant salt that will precipitate out when the concentrations of the species exceeds their respective solubility product. Thus Hydroxyapatite, $Ca_5(PO_4)_3(OH)$, is the calcium salt that will precipitate out and $MgHPO_4.3H_2O$ is the magnesium salt that will precipitate out.

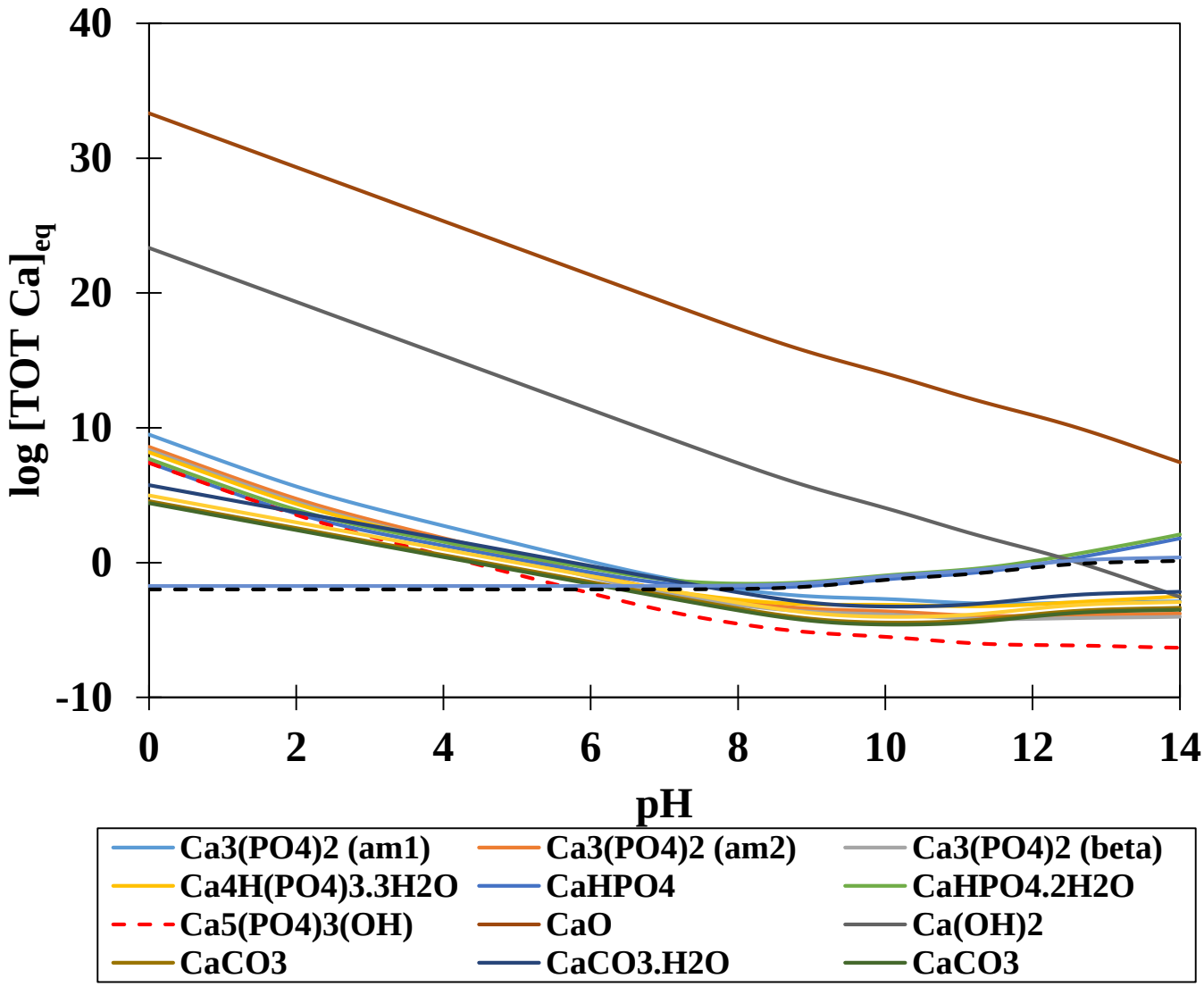

Figure 5: Solubility curves for {Ca^{2+} - PO_4^{3-}, CO_3^{2-}, SO_4^{2-}, Cl^-} solids. Assuming each solid precipitates individually; TOT [PO_4^{3-}]= 1.5 mg P/L; [CO_3^{2-}]= 1.2 g/L; [SO_4^{2-}]= 1 g/L; [Cl^-]= 2 g/L

Aqueous speciation for magnesium

Table 3: Stability constants for Mg- ligand complexes

	Metal ligand complexes	LogK
(i)	$Mg^{2+} + 2NH_4^+ \leftrightarrow Mg(NH_3)_2^{2+} + 2H^+$	-18.29
(ii)	$Mg^{2+} + H^+ + PO_4^{3-} \leftrightarrow MgHPO_{4(aq)}$	15.175
(iii)	$Mg^{2+} + H_2O \leftrightarrow MgOH^+ + H^+$	-11.417

(iv)	$Mg^{2+} + PO_4^{3-} \leftrightarrow MgPO_4^-$	12.9704
(v)	$Mg^{2+} + SO_4^{2-} \leftrightarrow MgSO_{4(aq)}$	2.26
(vi)	$Mg^{2+} + Cl^- \leftrightarrow MgCl^+$	0.6
(vii)	$Mg^{2+} + CO_3^{-2} \leftrightarrow MgCO_{3(aq)}$	2.92
(ix)	$Mg^{2+} + H^+ + CO_3^{2-} \leftrightarrow MgHCO_3^+$	11.34

$$[TOTMg]_{diss} = Mg^{2+} + Mg(NH_3)_2^{2+} + MgHPO_{4(aq)} + MgOH^+ MgPO_4^- + MgSO_{4(aq)} + MgCl^+ + MgCO_{3(aq)} + MgCO_{3(aq)} + MgHCO_3^+ \quad (19)$$

$$[TOTMg]_{diss} = Mg^{2+}\left\{1 + \frac{Mg(NH_3)_2^{2+}}{Mg^{2+}} + \frac{MgHPO_{4(aq)}}{Mg^{2+}} + \frac{MgOH^+}{Mg^{2+}} + \frac{MgPO_4^-}{Mg^{2+}} + \frac{MgSO_{4(aq)}}{Mg^{2+}} + \frac{MgCl^+}{Mg^{2+}} + \frac{MgCO_{3(aq)}}{Mg^{2+}} + \frac{MgHCO_3^+}{Mg^{2+}}\right\} \quad (30)$$

$$[TOTMg]_{diss} = Mg^{2+}\left\{1 + \frac{K_1(NH_4^+)^2}{(H^+)^2} + K_2(H^+)(PO_4^{3-}) + \left(\frac{K_3}{(H^+)}\right) + K_4(PO_4^{3-}) + K_5(SO_4^{2-}) + K_6(Cl^-) + K_7(CO_3^{-2}) + K_8(H^+)(CO_3^{-2}) + + \frac{K_9(NH_4^+)}{(H^+)}\right\} \quad (41)$$

Table 4: Ksp values for magnesium solids

	Equilibrium speciation for solids	$LogK_{sp}$
A	$Mg(OH)_2 + 2H^+ + \leftrightarrow Mg^{2+} + 2H_2O$	17.1
B	$Mg(OH)_{2(active)} + 2H^+ + \leftrightarrow Mg^{2+} + 2H_2O$	18.794
C	$Mg_3(PO_4)_2 \leftrightarrow 3Mg^{2+} + 2PO_4^{3-}$	-23.28
D	$MgHPO_4.3H_2O \leftrightarrow Mg^{2+} + H^+ + PO_4^{3-} + 3H_2O$	-18.175
E	$MgO + 2H^+ \leftrightarrow Mg^{2+} + H_2O$	21.584
F	$MgNH_4PO_4 \leftrightarrow Mg^{2+} + NH_4^+ + PO_4^{3-}$	-13.26
G	$Mg_2CO_3(OH)_2.3H_2O + 2H^+ \leftrightarrow 2Mg^{2+} + CO_3^{2-} + 5H_2O$	9.6
H	$Mg_5(CO_3)_4(OH)_2.4H_2O + 2H^+ \leftrightarrow 5Mg^{2+} + 4CO_3^{2-} + 6H_2O$	-8.766
I	$MgCO_3 \leftrightarrow Mg^{2+} + CO_3^{2-}$	-7.6
J	$Mg_2Cl(OH)_3.4H_2O + 3H^+ \leftrightarrow 2Mg^{2+} + Cl^- + 7H_2O$	26
K	$MgCO_3.5H_2O \leftrightarrow 2Mg^{2+} + CO_3^{2-} + 5H_2O$	-4.54
L	$MgCO_3.3H_2O \leftrightarrow Mg^{2+} + CO_3^{2-} + 3H_2O$	-4.67
M	$MgSO_4.7H_2O \leftrightarrow Mg^{2+} + SO_4^{2-} + 7H_2O$	-2.1265

$$Mg^{2+} = K_{sp1}(H^+)^2 \quad (52)$$

$$Mg^{2+} = K_{sp2}(H^+)^2 \quad (63)$$

$$Mg^{2+} = \left\{\frac{K_{sp3}}{(PO_4^{3-})^2}\right\}^{\frac{1}{3}} \quad (74)$$

$$Mg^{2+} = \frac{K_{sp4}}{(H^+)(PO_4^{3-})} \quad (85)$$

$$Mg^{2+} = K_{sp5}(H^+)^2 \quad (26)$$

$$Mg^{2+} = \frac{K_{sp6}}{(NH_4^+)(PO_4^{3-})} \quad (27)$$

$$Mg^{2+} = \left\{\frac{K_{sp7}}{(H^+)^2(CO_3^{2-})}\right\}^{\frac{1}{2}} \quad (28)$$

$$Mg^{2+} = \left\{\frac{K_{sp8}}{(H^+)^2(CO_3^{2-})^4}\right\}^{\frac{1}{5}} \quad (29)$$

$$Mg^{2+} = \frac{K_{sp9}}{CO_3^{2-}} \quad (30)$$

$$Mg^{2+} = \left\{\frac{K_{sp10}(H^+)^3}{Cl^-}\right\}^{\frac{1}{2}} \quad (91)$$

$$Mg^{2+} = \frac{K_{sp11}}{CO_3^{2-}} \quad (102)$$

$$Mg^{2+} = \frac{K_{sp12}}{CO_3^{2-}} \quad (113)$$

$$Mg^{2+} = \frac{K_{sp13}}{SO_4^{2-}} \quad (124)$$

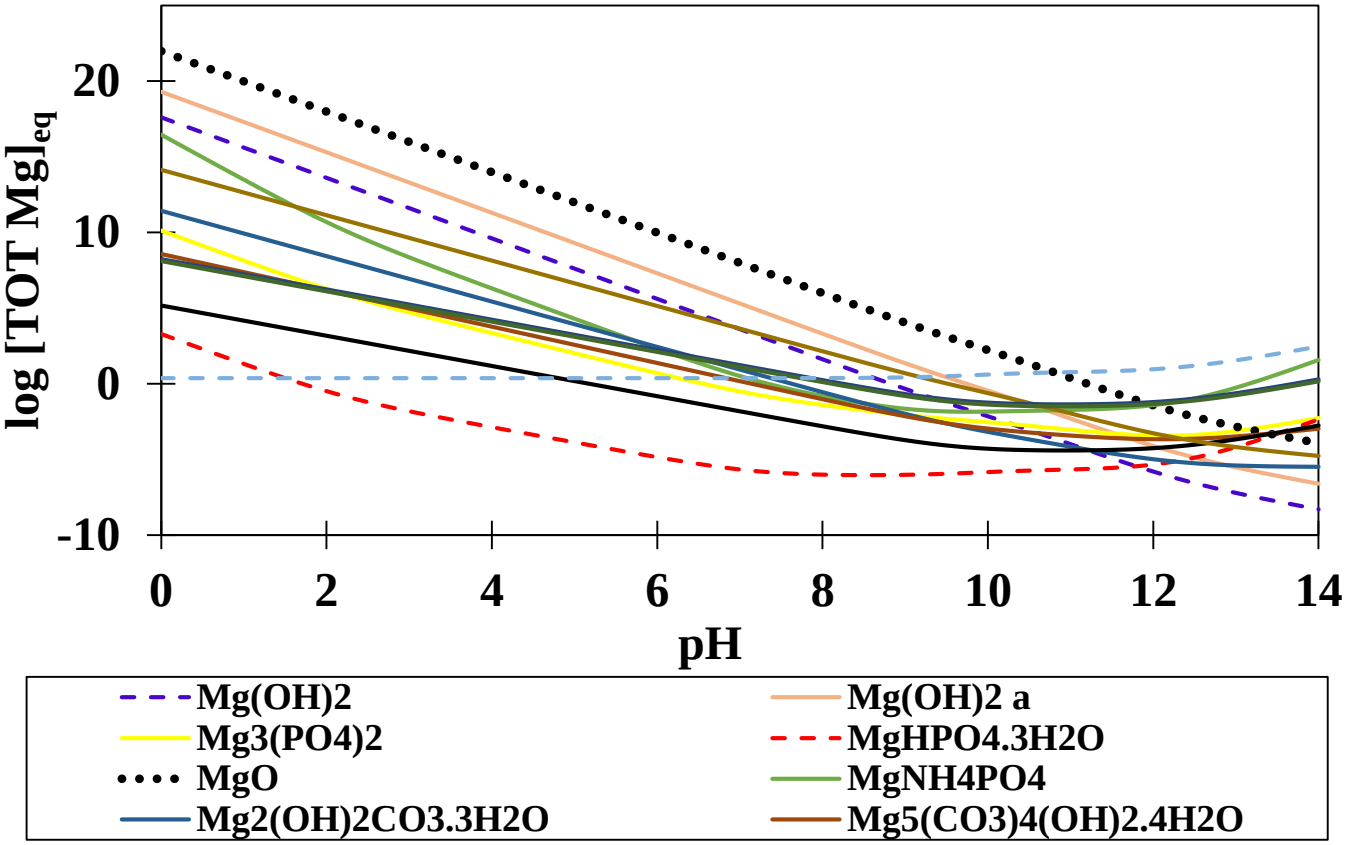

Figure 6: Solubility curves for {Mg^{2+} -PO_4^{3-}, CO_3^{2-}, SO_4^{2-}, Cl^-, NH_3} solids. Assuming each solid precipitates individually; TOT [PO_4^{-3}]= 1.5 mg P/L; [CO_3^{2-}]= 1.2 g/L; [SO_4^{2-}]= 1 g/L; [Cl^-]= 2 g/L

With the very high recovery that is achieved using iron oxides, our next goal will be to test the system for different types of reverse osmosis concentrates. We plan to test the system for the concentrate from Orange County Water District (OCWD). Further goals includes testing the reusability of the adsorbent and thus determining the number of cycles the adsorbent can be used for. Different concentrates have different types of contaminants, hence it will be interesting to see how the adsorption efficiency change for different water matrices.

Acknowledgement

We would like to thank the NWRI-SCSC for supporting our research.

References

- Boels, L.; Keesman, K.; and Witkamp, G., Adsorption of phosphonate antiscalant from reverse osmosis membrane concentrate onto granular ferric hydroxide. Environmental science & technology 46 (17) **2012**, 9638-9645.
- Cornell, R.; and Schwertmann, U. The iron oxides: structure, properties, reactions, occurrences, and uses; Wiley-VCH, Weinheim, 2nd, completely rev. and extended edition, 2003.
- Dadfarnia, S.; Haji Shabani, A.; Moradi, S.; Emami, S., Methyl red removal from water by iron based metal-organic frameworks loaded onto iron oxide nanoparticle adsorbent. Applied Surface Science 330, **2015**, 85-93.
- Geelhoed, J.; Hiemstra, T.; Riemsdijk, W. Phosphate and sulfate adsorption on goethite: Single anion and competitive adsorption. Geochim. Cosmochim. Acta, **1997**, 61 (12), 2389–2396.
- Genz, A. Entwicklung einer neuen Adsorptionstechnik zur Entfernung natürlicher Organika mit granuliertem Eisenhydroxid., Dissertation, Technische Universität Berlin, 2005.
- Jasinski, S. Phosphate Rock Reserves in the United States, Paper presented at the 2005 IFA Production and International Trade Conference, Sao Paolo, Brazil, September 11-14, 2005.
- Kayvani Fard, A.; Rhadfi, T.; Mckay, G.; Al-marri, M.; Abdala, A.; Hilal, N.; Hussien, M., Enhancing oil removal from water using ferric oxide nanoparticles doped carbon nanotubes adsorbents. Chemical Engineering Journal 293, **2016,** 90-101.
- Luo, Y.; Liu, L.; Qiao, W.; Liu, F.; Zhang, Y.; Tan, W.; Qiu, G., Facile crystal-structure-controlled synthesis of iron oxides for adsorbents and anode materials of lithium batteries. Materials Chemistry and Physics 170, **2016**, 239-245.
- Mohammadesmaeili, F.; Badr, M.; Abbaszadegan, M.; Fox, P. Mineral recovery from inland reverse osmosis concentrate using isothermal evaporation, Water Research, **2010**, 44 6021-6030.
- Runge-Metzger, A. Closing the cycle: obstacles to efficient P management for improved global food security. SCOPE 54 – Phosphorus in the Global Environment – Transfers, Cycles and Management. **1995**.